Journal of Hepatocellular Carcinoma Dovepress

Open Access Full Text Article ORIGINAL RESEARCH

Deep Learning-Based Automatic Segmentation Combined with Radiomics to Predict Post-TACE Liver Failure in HCC Patients

Shuai Li[1,*], Kaicai Liu[1,*], Chang Rong[1,*], Xiaoming Zheng[1], Bo Cao[2], Wei Guo[3], Xingwang Wu[1]

[1]Department of Radiology, the First Affiliated Hospital of AnHui Medical University, Hefei, Anhui Province, People's Republic of China; [2]Department of radiology, the Second affiliated hospital of NanJing Medical University, Nanjing, Jiangsu Province, People's Republic of China; [3]Department of Radiology, the Second Affiliated Hospital of ShanDong First Medical University, Taian, Shandong Province, People's Republic of China

*These authors contributed equally to this work

Correspondence: Xingwang Wu, Department of Radiology, The first affiliated hospital of AnHui medical university, No. 218 Jixi Road, Shushan District, Hefei, 230022, People's Republic of China, Email duobi2004@126.com

Objective: To develop and validate a deep learning-based automatic segmentation model and combine with radiomics to predict post-TACE liver failure (PTLF) in hepatocellular carcinoma (HCC) patients.

Methods: This was a retrospective study enrolled 210 TACE-trated HCC patients. Automatic segmentation model based on nnU-Net neural network was developed to segment medical images and assessed by the Dice similarity coefficient (DSC). The screened clinical and radiomics variables were separately used to developed clinical and radiomics predictive model, and were combined through multivariate logistic regression analysis to develop a combined predictive model. The area under the curve (AUC), calibration curve, and decision curve analysis (DCA) were applied to compare the performance of the three predictive models.

Results: The automatic segmentation model showed satisfactory segmentation performance with an average DSC of 83.05% for tumor segmentation and 92.72% for non-tumoral liver parenchyma segmentation. The international normalized ratio (INR) and albumin (ALB) was identified as clinically independent predictors for PTLF and used to develop clinical predictive model. Ten most valuable radiomics features, including 8 from non-tumoral liver parenchyma and 2 from tumor, were selected to develop radiomics predictive model and to calculate Radscore. The combined predictive model achieved the best and significantly improved predictive performance (AUC: 0.878) compared to the clinical predictive model (AUC: 0.785) and the radiomics predictive model (AUC: 0.815).

Conclusion: This reliable combined predictive model can accurately predict PTLF in HCC patients, which can be a valuable reference for doctors in making suitable treatment plan.

Keywords: hepatocellular carcinoma, TACE, liver failure, deep learning, radiomics

Introduction

Primary liver cancer (PLC) is one of the most common malignant tumors, ranking sixth in incidence and third in cancer-related mortality in the world,[1] and hepatocellular carcinoma (HCC) accounts for approximately 90% of PLC cases.[2] Due to its insidious onset and rapid progression, most patients are diagnosed with HCC at an advanced stage, with only 30–40% eligible for potentially curative treatments such as liver transplantation or hepatic resection.[3,4] For those unsuitable for surgical intervention, transarterial chemoembolization (TACE) has been recommended as a standard therapy by several guidelines,[5–7] as it is effective in controlling tumor growth, prolonging survival, and improving the quality of life for unresectable HCC patients. In addition, TACE also builds a bridge for connection with other therapies, such as hepatectomy[8] and targeted therapy.[9] A meta-analysis that included 101 papers with a total of 10,108 HCC cases noted that the objective remission rate after TACE is 52.5%, and the 1-year and 5-year overall survival (OS) rates are 70.3% and 32.4%, respectively, with a median OS of 19.4 months.[10] Nevertheless, TACE can lead to significant complications, with liver failure being one of the most severe and a common cause of mortality after TACE.[11] Approximately 7.5% (range: 0–48.6%) of patients experienced post-TACE

Received: 4 November 2024
Accepted: 7 December 2024
Published: 18 December 2024

liver failure (PTLF), with an associated mortality rate of 2.4% (range: 0–9.5%).[12] Although TACE is generally considered safe for patients with Child-Pugh class A or B liver function, liver failure still occurs in those patients, emphasizing the need for additional reliable predictors to diminish this risk.

Deep learning segmentation algorithms have shown significant promise in segmenting solid organs and tumors,[13–15] offering a robust tool for accurately distinguishing between non-tumoral liver parenchyma and tumors. Radiomics extracts a large volume of quantitative features from medical images, providing critical pathological and physiological insights that otherwise are unavailable through conventional imaging techniques and offering novel opportunities for disease diagnosis and prognosis.[16] Bernat[17] developed a predictive model by combining radiomics features and clinical risk scores to assess patients' response to TACE and overall survival, while Hu[18] successfully differentiated hepatic hemangiomas from HCC on CT images by radiomics and Zhao[19] integrated intra- and peri-tumoral radiomics features into a clinical-radiomics nomogram to predict post-TACE response in HCC patients. Furthermore, it has been demonstrated that there is a strong correlation between radiomics features, liver function and the biological behavior of tumors.[20] Therefore, we hypothesized that a radiomics model incorporating radiomics features of non-tumoral liver parenchyma and the tumor could be effective in predicting PTLF. To our knowledge, previous studies mainly focused on predicting post-hepatectomy liver failure or post-TACE treatment response,[21–23] Only a few studies have attempted to predict post-TACE liver failure (PTLF) using clinical or imaging features,[11,24] and no research has yet combined deep learning with radiomics for PTLF prediction.

Materials and Methods

Study Population

This retrospective study approved by the ethics committees of The First Affiliated Hospital of Anhui Medical University (Center 1, Research Ethics No: PJ2023-13-50) and the First Affiliated Hospital of University of Science and Technology of China (Center 2, Research Ethics No: 2023-RE-373), and conducted in accordance with the Declaration of Helsinki. Informed consent was waived. The study design is illustrated in Figure 1a, and the flow chart of the radiomics study is illustrated in Figure 1b. A total of 500 HCC patients treated with TACE between February 2018 and February 2024 in two centers were retrospectively reviewed. The inclusion criteria were as follows: radiologically or pathologically confirmed HCC; TACE as the initial treatment; complete abdominal imaging and laboratory examinations within one week prior to TACE, along with one month follow-up records post-operation. Exclusion criteria included extrahepatic metastases; ruptured HCC with bleeding; metastatic liver tumors; pre-TACE liver failure, and perioperative anticoagulant use. Finally, 147 patients from Center 1 (age range: 30–86, median age: 61) and 63 patients from Center 2 (age range: 28–86, median age: 59) were included in this study. Patients in Center 1 served as the training cohort and patients in Center 2 served as the validation cohort.

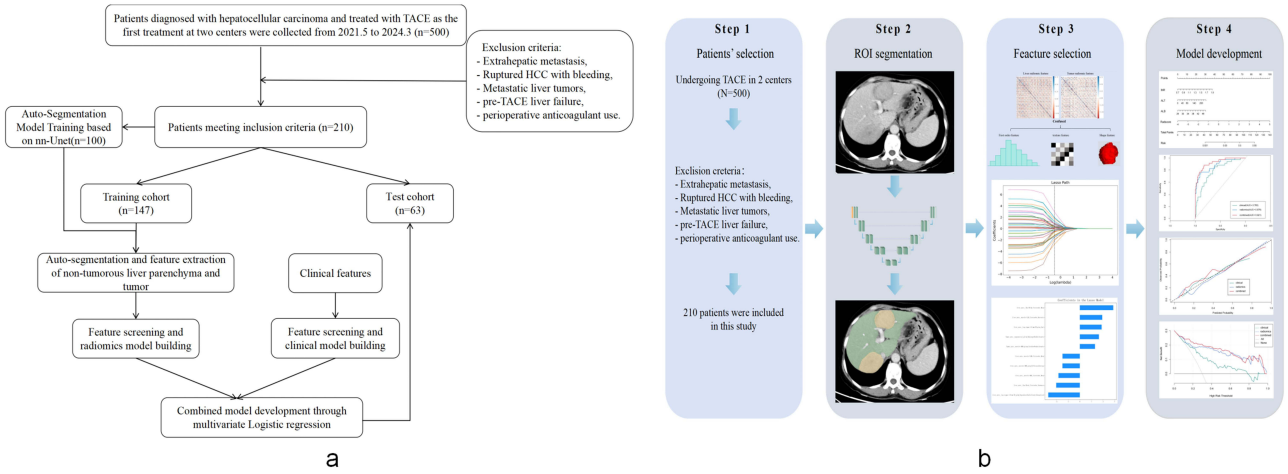

Figure 1 (**a**) The depict of study design (**b**) Flow chart of the radiomics study.

TACE Procedure

TACE procedure was conducted under local anesthesia using percutaneous femoral artery puncture, following the modified Seldinger technique. Superselective catheterization was performed via the right or left hepatic arteries, targeting tumor-feeding vessels under digital subtraction angiography (Allura Xper FD 20, Philips) guidance. Initial hepatic arteriography, utilizing a 5 Fr (RH or Yashiro) catheter, was employed to assess the tumor's location, size, number, and vascular supply. Iohexol or iodixanol was used as the contrast agent. Upon confirming the tumor-feeding artery, an iodized oil–chemotherapeutic agent emulsion (eg, piroxicam, raltitrexed, lopressor) was injected through a 2.7/2.8 Fr microcatheter. The dosage was determined based on tumor size and blood supply. Tumor vessels were embolized using gelatin sponges, polyvinyl alcohol (PVA) particles, or blank microspheres until blood flow ceased.

Diagnosis of PTLF

According to the 2019 Asia-Pacific Association for the Study of the Liver (APASL) consensus on acute-on-chronic liver failure (ACLF),[25] the diagnostic criteria for PTLF are as follows: jaundice (serum total bilirubin of 85 mmol/L or more), coagulation dysfunction (INR > 1.5 or PTA < 40%), and concomitant clinical ascites and/or hepatic encephalopathy within 4 weeks. PTLF was diagnosed when one of the above conditions was met.

Image Processing and Manual Segmentation

The CT scanning protocol is detailed in Supplementary Material 1. For volume of interest (VOI) segmentation, the intravenous phase images were selected, and the window level and window width were adjusted to 30 HU and 300 HU, respectively. Two radiologists (HYL with 7 years of experience and ZYJ with 5 years of experience in diagnostic abdominal imaging) manually segmented the non-tumoral liver parenchyma and tumor, layer by layer, using ITK-SNAP software (version 3.8.0; http://www.itksnap.org). A third radiologist, with 20 years of experience, reviewed all segmentations. To assess the intra- and inter-observer agreement, the two radiologists independently segmented the non-tumoral liver parenchyma and tumor for randomly selected 20 patients one week later.

Deep Learning-Based Automatic Segmentation Model

The nnU-Net is a deep-learning neural network for image segmentation,[26] which was designed to automatically configure the segmentation pipeline by analyzing the specific characteristics of biomedical segmentation task. This includes data pre-process, network architecture, and post-process. Our automatic segmentation model is based on 3D U-Net-like 22 architecture, composing of encoder and decoder paths, which are connected via skip connections, allowing for efficient feature extraction and reconstruction. In this study, the nnU-Net was utilized without any modification to segment the non-tumoral liver parenchyma and tumor in 3D. The nnU-Net architecture used in this study is illustrated in Figure 2. The code for nnU-Net is publicly available at https://github.com.

Predictive Model Development

The VOIs of non-tumoral liver parenchyma and tumors were obtained using the automatic segmentation model. Radiomic features, including the first-order features, texture features, and shape-based features, were extracted by the PyRadiomics package in Python. All the extracted features were Z-score normalized to eliminate dimensional differences before feature analysis. First, Spearman correlation analysis was used to exclude redundant features with intra-group correlation coefficients (ICC) >0.8. Then, features with P <0.05 were retained based on univariate analysis. Finally, the least absolute shrinkage and selection operator (LASSO) analysis was employed to select features with non-zero coefficients, and ten most valuable radiomics features were selected to calculate radiomics score (Radscore) for each patient and develop a radiomics predictive model.

Demographic characteristics and pre-treatment laboratory data of each patient were collected from the medical record system. The univariate analysis was used to identify factors associated with PTLF, and those factors with P <0.05 were further analyzed through multivariate logistic regression analysis to screen out the clinically independent predictors for PTLF, culminating in the development of a clinical predictive model.

A combined predictive model was developed by combining the Radscore and the clinically independent predictors through multivariate logistic regression analysis and visualized as a Clinical-Radiomics nomogram.

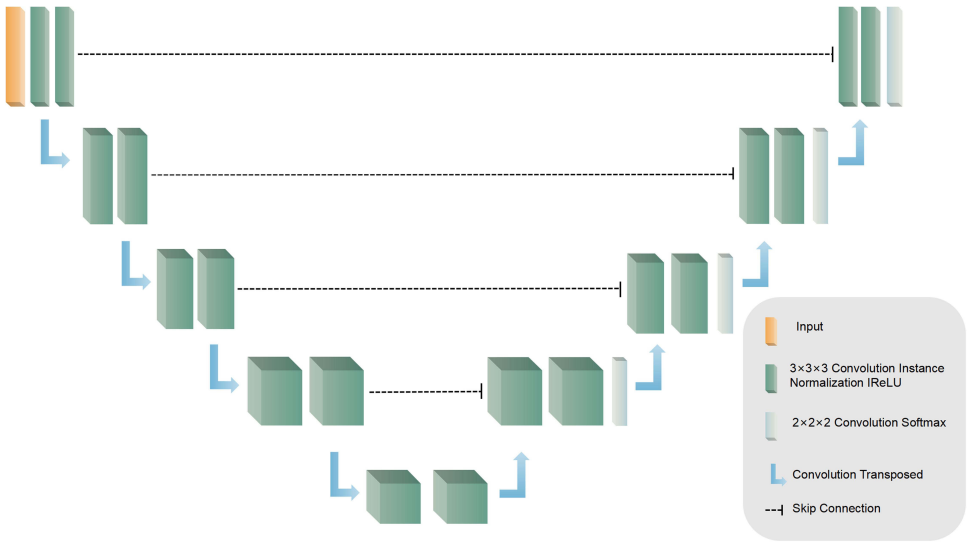

Figure 2 The network architecture of nnU-Net for non-tumoral liver parenchyma and tumor segmentation.

Statistical Analysis

SPSS 26.0 and R software (version 4.0.5) were used for data analyses. Normally and non-normally distributed continuous variables were analyzed using the *t*-test and Mann–Whitney *U*-test, respectively, with values expressed as mean ± standard deviation or median and interquartile range. Categorical variables were compared using chi-square tests, using numerical or percentage tables. Receiver operating characteristic (ROC) curves were used to evaluate the predictive performance of three models, and the area under the curve (AUC) was also calculated. Model accuracy and clinical utility were assessed through calibration curves and decision curve analysis (DCA). Differences in AUCs between the models were assessed using DeLong test. A two-sided of $P < 0.05$ was considered statistically different.

Results

Demographic Characteristics in the Segmentation Cohort and Categorized Dataset

The segmentation cohort is consisted of 100 HCC patients, including 32 patients with PTLF and 68 patients without PTLF. The demographic characteristics of the segmentation cohort is detailed in Supplementary Table 1. For the categorized dataset, PTLF occurred in 52 patients, 36 of whom were included in the training cohort and 16 in the validation cohort. The clinical and demographic characteristics of all patients in both the training and the validation cohorts are shown in Supplementary Table 2. No statistically significant differences were found between the training and the validation cohorts (all $P > 0.05$).

Development of Automatic Segmentation Model

We developed an automatic segmentation model based on the nnU-Net neural network using manually segmented VOIs of the non-tumoral liver parenchyma and the tumors of 100 HCC patients. The segment dataset was divided into 80 patients for training and validation sets and 20 patients for testing set. Results of the 5-fold cross-validation and the testing sets are presented in Table 1. The average DSC, accuracy, and recall were 83.05%, 92.15%, and 88.37% for the tumor segmentation and 92.72%, 92.65%, and 94.24% for the non-tumoral liver parenchyma segmentation, respectively. Supplementary Figure 1 gives two examples of automatic segmentation results for both tumor and non-tumoral liver parenchyma.

Development of Clinical Model, Radiomics Model and Combined Model

Univariate analysis based on the training cohort demonstrated that Neutrophil, RBC, ALB and INR were the clinical factors associated with PTLF (all $P < 0.05$) (Table 2). Multivariate analysis further indicated that INR (OR: 1992.169

Table 1 Automatic Segmentation Performance of the 5-Fold Cross-Validation and the Testing Sets

Metric	Object	Fold 0	Fold 1	Fold 2	Fold 3	Fold 4	Test
DICE(%)	Liver	94.58	87.30	93.81	94.59	93.33	94.00
	Tumor	79.79	85.18	85.39	86.15	78.76	85.06
Jaccard(%)	Liver	89.80	81.92	88.44	89.78	87.56	88.83
	Tumor	70.00	78.53	75.25	76.43	69.13	75.98
Precision(%)	Liver	94.17	90.35	92.21	94.39	92.15	93.67
	Tumor	91.45	91.88	93.30	92.05	92.05	93.47
Recall(%)	Liver	95.26	91.05	95.30	94.98	94.63	94.77
	Tumor	87.07	94.33	83.89	87.69	88.85	93.25

Table 2 Univariate Analysis Based on the Training Cohort

Characteristics	PTLF(n=36)	NPTLF(n=111)	*P*
Sex(Male/Female)	32/4	96/15	0.709
Age(year)	59.00(51.00, 70.00)	63.00(53.00,70.00)	0.556
Tumor location(n%)			0.641
Right lobe	30(83.40)	93(84.50)	
Left lobe	3(8.30)	13(11.00)	
Right and Left lobe	3(8.30)	5(4.50)	
Number of tumors(n%)			0.378
1	24(66.70)	61(55.00)	
≥2	12(33.30)	50(45.00)	
Sun of tumor diameters(cm)	9.41(4.40, 14.39)	9.68(6.04, 14.41)	0.681
Liver cirrhosis(n%)	24(66.70)	64(57.70)	0.338
Hydroperitoneum(n%)	9(25.00)	26(23.40)	0.847
WBC($\times10^9$)	4.48(3.27, 6.26)	5.71(3.92, 6.96)	0.069
Neutrophil(n%)	63.35(56.00,68.78)	66.40(60.40, 74.10)	0.041
RBC($\times10^{12}$)	4.37(3.84, 4.86)	4.03(3.60, 4.47)	0.017
Hb(g/l)	131.33 ± 23.70	124.41 ± 23.14	0.131
ALB(g/l)	40.48 ± 7.74	37.05 ± 4.77	<0.01
PLT($\times10^{12}$)	128.50(97.75, 211.00)	151.00(92.00, 204.00)	0.783
PT(s)	13.15(12.00, 14.13)	12.60(11.80, 14.00)	0.345
TT(s)	17.95(16.83, 19.00)	18.30(16.90, 19.50)	0.341
INR	1.21(1.07, 1.29)	1.01(0.94, 1.10)	<0.01
APTT(s)	31.00(27.13, 37.80)	29.50(26.90, 35.70)	0.257
AST(IU/L)	53.00(34.93, 85.00)	55.00(33.00, 81.00)	0.887
ALT(IU/L)	54.00(24.20, 111.75)	40.00(23.00, 65.00)	0.154
TB(umol/L)	16.80(13.73, 23.85)	19.30(15.00, 24.10)	0.198
GLU(mmol/L)	4.97(4.33, 5.82)	5.07(4.48, 5.66)	0.792
GGT(IU/L)	119.50(70.00, 229.25)	120.30(69.00, 255.00)	0.729
AFP(ng/mL)	219.24(10.14, 2942.00)	221.50(16.40, 1594.32)	0.866
Embolus(n%)	11(30.60)	45(40.54)	0.284
CTP(n%)			0.853
Class A	30(83.30)	91(82.00)	
Class B	6(17.60)	20(18.00)	

Abbreviations: PTLF, post-TACE liver failure; NPTLF, non-post-TACE liver failure; WBC, white blood cell; RBC, red blood cell; Hb, hemoglobin; ALB, albumin; PLT, platelet count; PT, prothrombin time; TT, thrombin time; INR, international standardized ratio; APTT, activated partial thromboplastin time; AST, glutamate transaminase; ALT, alanine aminotransferase; TB, total bilirubin; GLU, glucose; GGT, gamma-glutamyl transferase; AFP, alpha-fetoprotein; CTP, Child-Turcotte-Pugh.

Table 3 Multivariate Analysis Based on the Training Cohort

variables	β	Odds ratio(95% CI)	*P*
Neutrophil(n%)	0.124	1.014 (0.743, 1.962)	0.463
RBC($\times 10^{12}$)	0.273	1.314 (0.703, 2.456)	0.392
ALB	0.163	1.117 (1.043, 1.327)	<0.01
INR	7.597	1992.169 (46.629, 85,113.563)	<0.01
Radscore	0.317	1.373 (1.190, 1.584)	<0.01

Abbreviations: OR, odds ratio; CI, confidence interval; ALB, albumin; RBC, red blood cell; INR, international standardized ratio.

(95% CI: 46.629, 85,113.563, $P \leq 0.01$)) and ALB (OR: 1.117 (95% CI: 1.043, 1.327, $P \leq 0.01$)) were the clinically independent predictors of PTLF (Table 3), resulting in the development of a clinical predictive model.

A total of 1874 radiomics features were separately extracted from the non-tumoral liver parenchyma and the tumor of each HCC patient, and those two sets of radiomics features were fused together for analysis. All extracted features were Z-score normalized before radiomics analysis. Of the 3748 radiomics features, 410 features remained following the removal of redundant features (ICC > 0.8) using Spearman correlation analysis; 45 radiomics features with non-zero coefficients were screened out through univariate and LASSO analyses (Figure 3a); the top 10 radiomics features with the highest weights (Figure 3b) were selected for the multivariate logistic regression analysis to develop a radiomics predictive model. As detailed in Supplementary Material 2, the Radscore of each patient was calculated by multiplying the selected features by a linear combination of their respective coefficients.

Finally, a combined predictive model was developed by combining the ALB, INR and the Radscore through multivariate logistic regression analysis.

Model Comparison and Nomogram Development

Model comparisons were all conducted in the validation cohort. The ROC curves of the three predictive models are shown in Figure 4a, and the combined predictive model (AUC: 0.878, 95% CI: 0.761, 0.994) exhibited the best discrimination power between PTLF and non-PTLF patients compared to the clinical predictive model (AUC: 0.785, 95% CI: 0.653, 0.916) and the radiomics predictive model (AUC: 0.815, 95% CI: 0.690, 0.940). The DCA (Figure 4b) further demonstrated that the combined predictive model provided a greater net clinical benefit in the 0.1–0.95 risk threshold. Additionally, as shown in Figure 4c and d, the combined model showed good consistency between predicted and actual probabilities in both the training and the validation cohorts. Above results confirmed the superiority of the combined predictive model. Thus, we visualized the combined predictive model as a nomogram for clinical application (Figure 5). Supplementary Figure 2 shows an example of using a nomogram for the risk prediction of PTLF.

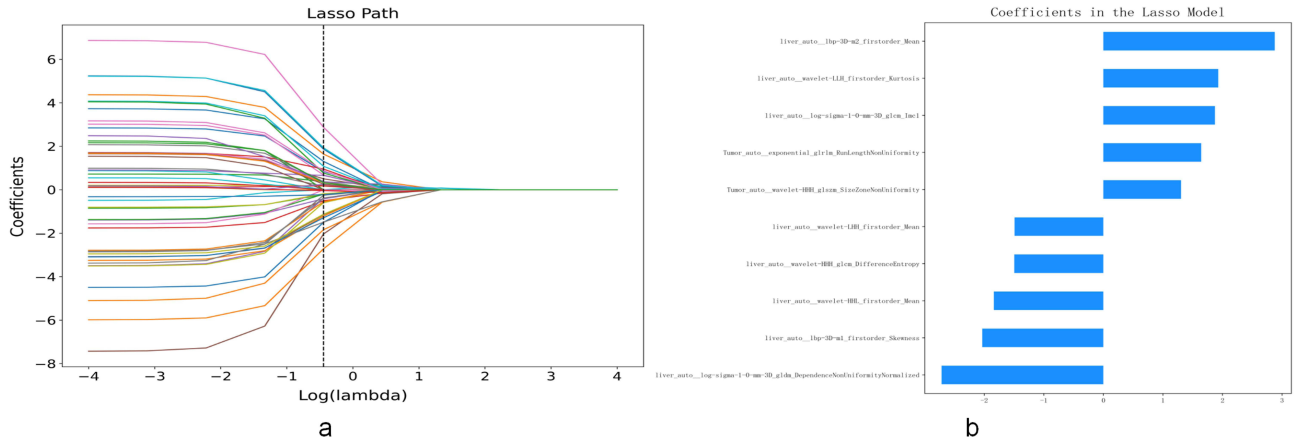

Figure 3 (**a**) LASSO path of radiomics. (**b**) Selected radiomics features and their corresponding weights.

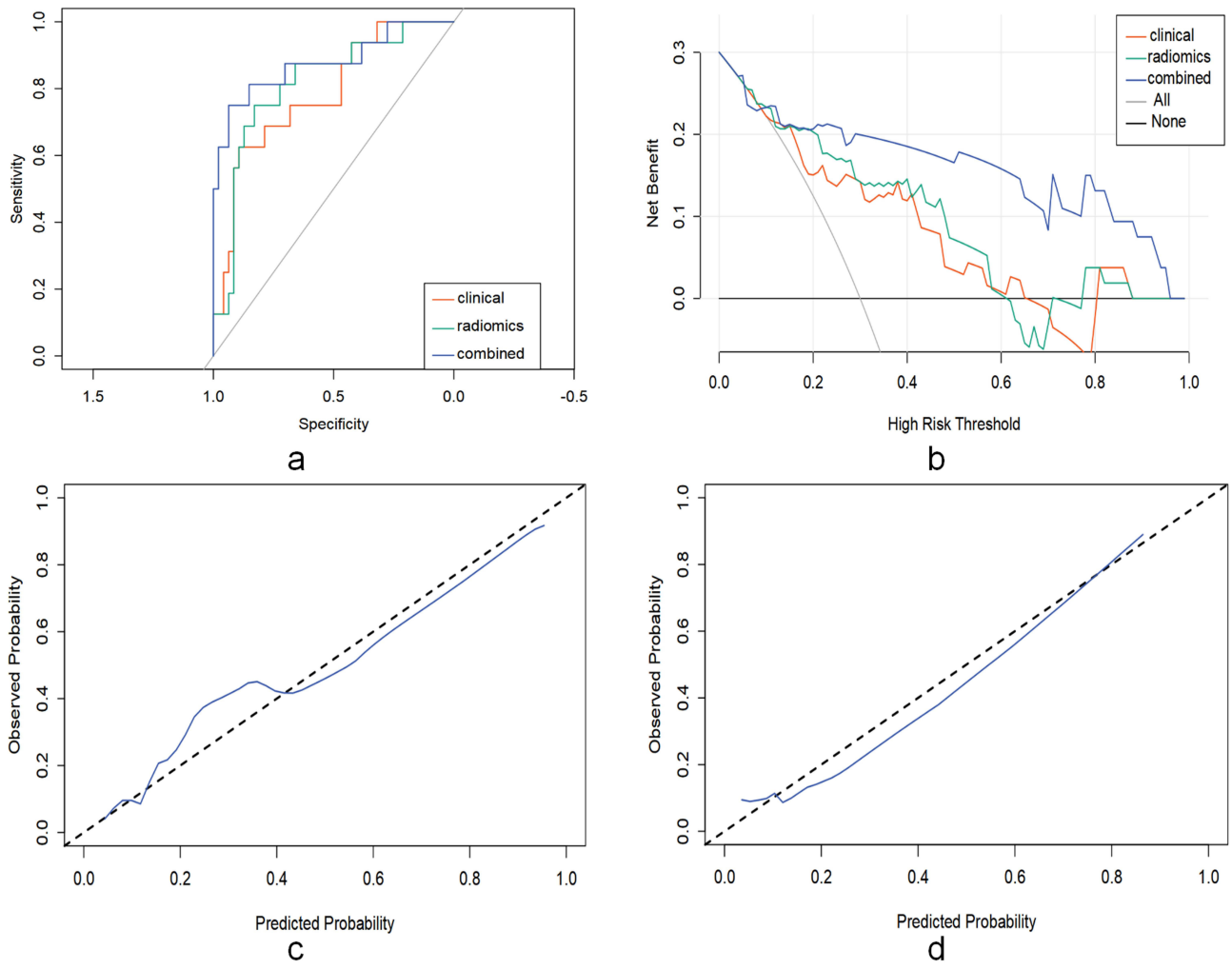

Figure 4 (**a**) ROC curves for the three models in the validation cohort. (**b**) DCA for the three models in the validation cohort. (**c**) Calibration curve of the combined model in the training cohort. (**d**) Calibration curve of the combined model in the validation cohort.

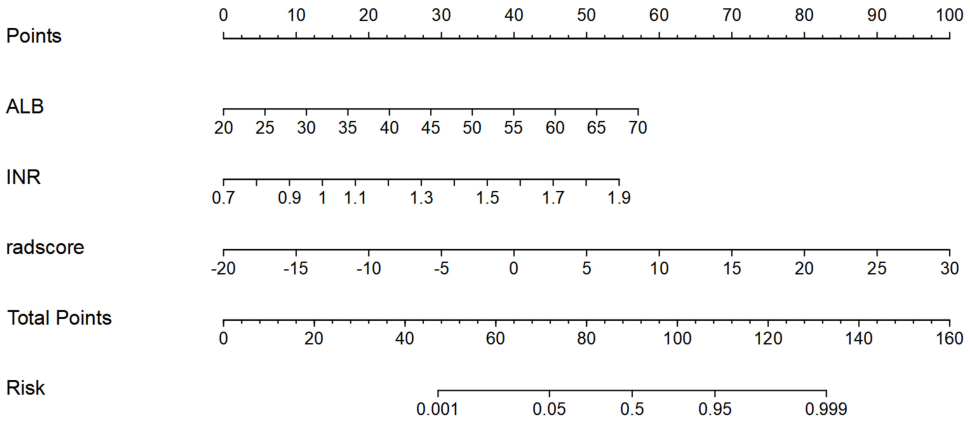

Figure 5 Clinical-Radiomics nomogram.

Discussion

Previous study has indicated that PTLF is an independent risk factor for the lower survival rate of liver cancer patients.[27] Hence, an effective mean to predict PTLF is of great importance. Our study demonstrated that a radiomics model, which

integrates radiomics features of the non-tumoral liver parenchyma and tumor for fusion analysis, can effectively predict PTLF in HCC patients prior to TACE. On the one hand, the incorporation of clinical factors further improved the predictive performance; on the other hand, the deep learning-based automatic segmentation techniques enhanced the clinical utility of this predictive model. This valuable and reliable predictive model can assists clinicians identify PTLF risk at an early stage, allowing timely adjustments of treatment plan.

Yang et al[11] developed a mathematical model based on clinical risk factors to predict PTLF. However, their model could not be used alone to exclude patients for TACE because of the low positive predictive value (28.9%). Radiomics provides a powerful method for extracting information that beyond the perception of the human eyes and enables the assessment of tumor biology features and prognosis.[28] Some research has demonstrated the utility of radiomics in predicting liver failure after hepatectomy[29] and post-TACE response in HCC patients.[30,31] It confirmed the feasibility of radiomics in predicting PTLF. However, they all use manual segmentation or semiautomatic segmentation of the ROI, which brings some obstacles to clinical application. In our study, we integrated automatic segmentation into the radiomics study, which significantly reduced labor work and potential human error. The nnU-Net-based automatic segmentation model that developed in our study reduced the segmentation task for 100 HCC cases from 10 days to a few minutes with high accuracy (average DSC: 83.05% for tumor segmentation and 92.72% for non-tumoral liver parenchyma segmentation), highlighting its efficiency and reliability compared to the traditional manual segmentation, which is time-consuming and prone to variability. In our study, the DCS of this automatic segmentation model for tumor segmentation was lower than that of non-tumoral liver parenchyma segmentation, it may be attributed to the blurred boundaries of tumors and confusion with surrounding tissues, which makes tumor segmentation on CT images relatively difficult, and the heterogeneity of tumors in terms of morphology and density increased the complexity of tumor segmentation. In addition, the 5-mm layer thickness of CT images may result in loss of detail, especially affecting smaller tumors with blurred borders, whereas non-tumoral liver parenchyma is less sensitive to resolution changes due to its larger area.

In our study, 8 radiomics features extracted from non-tumoral liver parenchyma and 2 radiomics features extracted from tumor were selected as the most valuable features to develop radiomics predictive model. As shown in Figure 3b, the non-tumoral liver parenchyma features have a greater weight in the model, indicating that the non-tumoral liver injury, rather than tumor necrosis, is the main contributor to PTLF, and it aligns with the previous research[32]. This may be related to TACE-induced cytolysis.[33]

In order to improve the predictive performance of the radiomics predictive model, we further introduced clinical predictors that were highly correlated with PTLF into the radiomics predictive model. In our study, INR, and ALB were identified as clinically independent predictors for PTLF, which is consistent with previous studies.[34,35] INR is the standardized display of the results of PT, which is one of the most commonly used indicators of the body's coagulation function, and ALB is the performer of many important functions in the body, such as maintaining colloid osmotic pressure and transporting various substances. Since the liver synthesizes all of the ALB and most of the clotting factors in the body, the basal levels of both are directly proportional to the number of normal hepatocytes. Although TACE targets selective embolization of tumor-feeding vessels, it inevitably causes ischemic damage to some normal liver parenchyma. Lower preoperative ALB and higher INR indicate fewer healthy liver cells, making patients more susceptible to PTLF. This supports the view that liver function decompensation and failure post-TACE are due to non-tumoral liver injury rather than tumor necrosis, too.[33]

The addition of clinical factors into radiomics predictive model resulted in a combined model with superior predictive performance, as proved by its higher AUC(0.878) compared to the radiomics model (AUC: 0.815), and the DeLong test showed that there is a statistically significant difference between the AUCs of the two models ($P<0.05$). Additionally, DCA demonstrated that the combined model offered greater net benefit across a wide range of risk threshold, affirming its better clinical utility. Another study[36] indicated that the PCCA variant rs16957301 was specifically associated with acute kidney injury in cancer patients after immune checkpoint inhibitors (ICIs) treatment and could serve as an significant predictor. Moreover, their findings highlighted the need to consider racial, ethnic, and genetic diversity in patients' responses to ICI treatment. Similarly, is PTLF associated with genetic variation, race, ethnicity, and genetic diversity? More and larger studies are needed to confirm this in the future.

Our study has some limitations. First, the low incidence of PTLF[9] limited the sample size, which may introduce inherent biases and hidden confounding factors. Additionally, most patients received concurrent systemic therapies after

TACE, and we did not account for variables such as drug type and dosage, which may impact the onset of PTLF. Lastly, our study followed a two-step process involving segmentation and prediction, and future research should explore the incorporation of deep learning methods for end-to-end risk prediction.

Conclusion

This combined predictive model proves to be a valuable tool for predicting PTLF. It can assist clinicians in conducting early intervention for patients at high risk of PTLF and improve the prognosis of HCC patients treated with TACE.

Funding

This work is supported by the Natural Science Fundation of Anhui Province (2308085MH241) and the Research Funds for Academic and Technological Leaders in Anhui Province of China (2021D299).

Disclosure

The authors declare that they have no competing interests.

References

1. Sung H, Ferlay J, Siegel RL, et al. Global cancer statistics 2020: GLOBOCAN estimates of incidence and mortality worldwide for 36 cancers in 185 countries. *CA*. 2021;71(3):209–249. doi:10.3322/caac.21660
2. Pagano D, Khouzam S, Magro B, et al. How important is the role of iterative liver direct surgery in patients with hepatocellular carcinoma for a transplant center located in an area with a low rate of deceased donation? *Front Oncol*. 2022;12:929607. doi:10.3389/fonc.2022.929607
3. Raoul J-L, Forner A, Bolondi L, et al. Updated use of TACE for hepatocellular carcinoma treatment: how and when to use it based on clinical evidence. *Cancer Treat Rev*. 2019;72:28–36. doi:10.1016/j.ctrv.2018.11.002
4. Pinna AD, Yang T, Mazzaferro V, et al. Liver transplantation and hepatic resection can achieve cure for hepatocellular carcinoma. *Ann Surg*. 2018;268(5):868–875. doi:10.1097/SLA.0000000000002889
5. European Association for the Study of the Liver. Electronic address: easloffice@easloffice.eu. and European Association for the Study of the Liver. EASL clinical practice guidelines: management of hepatocellular carcinoma. *J Hepatol*. 2018;vol. 69(1):182–236. doi:10.1016/j.jhep.2018.03.019
6. Zhou J, Sun H, Wang Z, et al. Guidelines for the diagnosis and treatment of hepatocellular carcinoma (2019 Edition). *Liver Cancer*. 2020;9 (6):682–720. doi:10.1159/000509424
7. Reig M, Forner A, Rimola J, et al. BCLC strategy for prognosis prediction and treatment recommendation: the 2022 update. *J Hepatol*. 2022; vol. 76(3):681–693. doi:10.1016/j.jhep.2021.11.018
8. Goumard C, Komatsu S, Brustia R, et al. Technical feasibility and safety of laparoscopic right hepatectomy for hepatocellular carcinoma following sequential TACE-PVE: a comparative study. *Surg Endosc*. 2017;vol. 31(5):2340–2349. doi:10.1007/s00464-016-5225-y
9. Lencioni R, Llovet JM, Han G, et al. Sorafenib or placebo plus TACE with doxorubicin-eluting beads for intermediate stage HCC: the SPACE trial. *J Hepatol*. 2016;vol. 64(5):1090–1098. doi:10.1016/j.jhep.2016.01.01
10. Lencioni R, de Baere T, Soulen MC, et al. Lipiodol transarterial chemoembolization for hepatocellular carcinoma: a systematic review of efficacy and safety data. *Hepatology*. 2016;vol. 64(1):106–116. doi:10.1002/hep.28453
11. Min YW, Kim J, Kim S, et al. Risk factors and a predictive model for acute hepatic failure after transcatheter arterial chemoembolization in patients with hepatocellular carcinoma. *Liver Int*. 2013;vol. 33(2):197–202. doi:10.1111/liv.12023
12. Marelli L, Stigliano R, Triantos C, et al. Transarterial therapy for hepatocellular carcinoma: which technique is more effective? A systematic review of cohort and randomized studies. *Cardiovascu Interv Radiol*. 2007;30(1):6–25. doi:10.1007/s00270-006-0062-3
13. Gul S, Khan MS, Bibi A, et al. Deep learning techniques for liver and liver tumor segmentation: a review. *Comput Biol Med*. 2022;147:105620. doi:10.1016/j.compbiomed.2022.105620
14. Yuchun L, Wu Y, Huang M, et al. Attention-guided multi-scale learning network for automatic prostate and tumor segmentation on MRI. *Comput Biol Med*. 2023;165:107374. doi:10.1016/j.compbiomed.2023.107374
15. Zhao Z, Chen H, Li J, Wang L.Boundary attention u-net for kidney and kidney tumor segmentation. Annual International Conference of the IEEE Engineering in Medicine and Biology Society. IEEE Engineering in Medicine and Biology Society. Annual International Conference. 2022 2022: 1540–1543. doi:10.1109/EMBC48229.2022.9871443.
16. Lambin P, Rios-Velazquez E, Leijenaar R, et al. Radiomics: extracting more information from medical images using advanced feature analysis. *Eur J Cancer*. 2012;48(4):441–446. doi:10.1016/j.ejca.2011.11.036
17. Bernatz S, Elenberger O, Ackermann J, et al. CT-radiomics and clinical risk scores for response and overall survival prognostication in TACE HCC patients. *Sci Rep*. 2023;13(1):533. doi:10.1038/s41598-023-27714-0
18. Shuyi H, Lyu X, Li W, et al. Radiomics analysis on noncontrast CT for distinguishing hepatic hemangioma (HH) and hepatocellular carcinoma (HCC). *Contrast Media Mol Imaging*. 2022;2022(1):7693631. doi:10.1155/2022/7693631
19. Zhao Y, Zhang J, Wang N, et al. Intratumoral and peritumoral radiomics based on contrast-enhanced MRI for preoperatively predicting treatment response of transarterial chemoembolization in hepatocellular carcinoma. *BMC Cancer*. 2023;23(1):1026. doi:10.1186/s12885-023-11491-0
20. Schobert IT, Savic LJ, Chapiro J, Zhang X, Liu Y, Geschwind JF. Radiomics-based machine learning analysis for prediction of hepatocellular carcinoma response to transarterial chemoembolization: a proof-of-concept study. *J Vasc Interv Radiol*. 2020;31(6):1006–1014.
21. Peng Y, Shen H, Tang H, et al. Nomogram based on CT-derived extracellular volume for the prediction of post-hepatectomy liver failure in patients with resectable hepatocellular carcinoma. *Eur Radiol*. 2022;32(12):8529–8539. doi:10.1007/s00330-022-08917-x

22. Shi Z-X, Li C-F, Zhao L-F, et al. Computed tomography radiomic features and clinical factors predicting the response to first transarterial chemoembolization in intermediate-stage hepatocellular carcinoma. *Hepatobiliary Pancreat Dis Int*. 2024;23(4):361–369. doi:10.1016/j.hbpd.2023.06.011
23. Niu X-K, Xiao-Feng H. Development of a computed tomography-based radiomics nomogram for prediction of transarterial chemoembolization refractoriness in hepatocellular carcinoma. *World J Gastroenterol*. 2021;27(2):189–207. doi:10.3748/wjg.v27.i2.189
24. Yuan M, Chen T-Y, Chen X-R, et al. Identification of predictive factors for post-transarterial chemoembolization liver failure in hepatocellular carcinoma patients: a retrospective study. *World J Clin Cases*. 2022;10(24):8535–8546. doi:10.12998/wjcc.v10.i24.8535
25. Sarin SK, Choudhury A, Sharma MK, et al. Acute-on-chronic liver failure: consensus recommendations of the Asian Pacific association for the study of the liver (APASL): an update. *Hepatol Internat*. 2019;13(4):353–390. doi:10.1007/s12072-019-09946-3
26. Isensee F, Jaeger PF, Kohl SAA, et al. nnU-Net: a self-configuring method for deep learning-based biomedical image segmentation. *Nature Methods*. 2021;18(2):203–211. doi:10.1038/s41592-020-01008-z
27. Hsin I-F, Hsu C-Y, Huang H-C, et al. Liver failure after transarterial chemoembolization for patients with hepatocellular carcinoma and ascites: incidence, risk factors, and prognostic prediction. *J Clin Gastroenterol*. 2011;45(6):556–562. doi:10.1097/MCG.0b013e318210ff17
28. Liu Z, Wang S, Dong D, et al. The applications of radiomics in precision diagnosis and treatment of oncology: opportunities and challenges. *Theranostics*. 2019;9(5):1303–1322. PMID: 30867832; PMCID: PMC6401507. doi:10.7150/thno.30309
29. Cai W, He B, Hu M, et al. A radiomics-based nomogram for the preoperative prediction of posthepatectomy liver failure in patients with hepatocellular carcinoma. *Surg Oncol*. 2019;28:78–85. PMID: 30851917. doi:10.1016/j.suronc.2018.11.013
30. Chen M, Cao J, Hu J, et al. Clinical-radiomic analysis for pretreatment prediction of objective response to first transarterial chemoembolization in hepatocellular carcinoma. *Liver Cancer*. 2021;10(1):38–51. doi:10.1159/000512028
31. Kong C, Zhao Z, Chen W, et al. Prediction of tumor response via a pretreatment MRI radiomics-based nomogram in HCC treated with TACE. *Eur Radiol*. 2021;31(10):7500–7511. doi:10.1007/s00330-021-07910-0
32. Arroyo V, García-Martinez R, Salvatella X, et al. Human serum albumin, systemic inflammation, and cirrhosis. *J Hepatol*. 2014;61(2):396–407. doi:10.1016/j.jhep.2014.04.012
33. Paye F, Farges O, Dahmane M, et al. Cytolysis following chemoembolization for hepatocellular carcinoma. *Br J Surg*. 1999;86(2):176–180. doi:10.1046/j.1365-2168.1999.01014.x
34. Silva ANS, Greensmith M, Praseedom RK, et al. Early derangement of INR predicts liver failure after liver resection for hepatocellular carcinoma *Surgeon*. 2022;20(5):e288–e295. doi:10.1016/j.surge.2022.01.002
35. Lee K-H, Tse M-LD, Law M, et al. Development and validation of an imaging and clinical scoring system to predict early mortality in spontaneous ruptured hepatocellular carcinoma treated with transarterial embolization. *Abdom Radiol*. 2019;44(3):903–911. doi:10.1007/s00261-019-01895-7
36. Wang Y, Xiong C, Yu W, et al. PCCA variant rs16957301 is a novel AKI risk genotype-specific for patients who receive ICI treatment: real-world evidence from all of us cohort. *Eur J Cancer*. 2024:115114. doi:10.1101/2024.06.20.24309197